the FEBS Journal

Robust and flexible response of the *Ostreococcus tauri* circadian clock to light/dark cycles of varying photoperiod

Quentin Thommen[1], Benjamin Pfeuty[1], Florence Corellou[2], François-Yves Bouget[2] and Marc Lefranc[1]

1 Laboratoire de Physique des Lasers, Atomes, et Molécules, Université Lille 1, CNRS, Unité Mixte de Recherche 8523, Unité de Formation et de Recherche de Physique, Villeneuve d'Ascq, France
2 Laboratoire d'Océanographie Microbienne, Université Pierre et Marie Curie (Paris 6), CNRS, Unité Mixte de Recherche 7621, Observatoire Océanologique de Banyuls, Avenue du Fontaulé, Banyuls sur Mer, France

Keywords
circadian clocks; entrainment; flexibility; *Ostreococcus tauri*; robustness

Correspondence
M. Lefranc, Laboratoire de Physique des Lasers, Atomes, et Molécules, Université Lille 1, Centre National de la Recherche Scientifique, Unité Mixte de Recherche 8523, Unité de Formation et de Recherche de Physique, F-59655 Villeneuve d'Ascq, France
Fax: +33 320 337020
Tel: +33 320 336450
E-mail: marc.lefranc@univ-lille1.fr

(Received 19 December 2011, revised 19 April 2012, accepted 24 May 2012)

doi:10.1111/j.1742-4658.2012.08666.x

The green microscopic alga *Ostreococcus tauri* has recently emerged as a promising model for understanding how circadian clocks, which drive the daily biological rhythms of many organisms, synchronize to the day/night cycle in changing weather and seasons. Here, we analyze translational reporter time series data for the central clock genes *CCA1* and *TOC1* for a wide range of daylight durations (photoperiods). The variation of temporal expression profiles with day duration is complex, with the two protein peaks tracking different times of the day. Nevertheless, all profiles are accurately reproduced by a simple two-gene transcriptional loop model whose parameters depend on light only through the photoperiod value. We show that this non-intuitive behavior allows the circadian clock to combine flexibility and robustness with respect to daylight fluctuations.

Introduction

Most cellular functions are controlled by complex networks of molecular interactions that routinely achieve sophisticated information processing and decision making. These networks, featuring manifold feedback and feed-forward regulations, display a highly non-linear collective dynamics [1–3]. In addition to reproducing observations and checking the consistency of a biological hypothesis, mathematical modeling is essential for identifying the design principles at work in cellular machinery [4]. For example, it has been proposed that the oscillatory behavior of the NF-κB transcription factor is key to its ability to integrate cellular signals of various origins and channel them to the appropriate target [5,6].

However, such modeling requires taking into account the constraints under which the molecular network studied has evolved [7]. Most importantly, cells not only have to generate an appropriate response to a given signal, but to do so under predictably or unpredictably varying conditions, while maintaining exquisite sensitivity. The combined requirements of robustness and flexibility have undoubtedly shaped the architecture of cell molecular networks. Accordingly, mathematical modeling has been harnessed to obtain insight into the dynamic ingredients underlying such properties that make circuits in living cells so different from a random dynamic system [8–11].

Abbreviations
FRP, free-running period; iPRC, impulse phase response curve; RMS, root mean square; ZT, Zeitgeber time.

In this respect, circadian biology is a promising field [12–14]. Circadian clocks have a well-defined function: they keep the time of day so that the daily changes in the environment caused by the Earth's rotation can be anticipated [15,16]. These biochemical oscillators, comprising genes and proteins that interact so as to generate oscillations with a period of ~ 24 h, precisely synchronize with the day/night cycle so that stable and regular molecular ticks are scheduled. Delivering such signals in the fluctuating environment of a cell is a formidable challenge in itself, but this task is further complicated by the fact that different expression profiles must be generated as the day/night cycle varies across the year [17–23], with short days in winter and long days in summer, in order to track important moments of the day [24–26]. Fortunately, while understanding clock robustness is a difficult problem, assessing it only requires monitoring of the circadian oscillator phase.

To understand the behavior of a functional circadian clock, the autonomous biochemical oscillator must be considered together with the day/night cycle driving it, as it is this interaction that ensures precise time-keeping. The forcing is generally parametric: one or several parameters of the internal oscillator are modulated by the external cycle, with daylight being the principal cue. For example, a clock protein may be degraded faster in the light [27,28] or in the dark [29].

This biochemical action of light on one or several kinetic parameters of the clock, which couples the dynamics of the circadian clock to that of the day/night cycle, is referred to as 'coupling'. For strong enough coupling, the phenomenon of entrainment is observed: the period of the oscillator is locked exactly to that of the external forcing, ensuring that a 24 h rhythm is generated, and a definite phase relationship between the two cycles is maintained [30–34].

Thus, understanding circadian clock robustness requires identification of the ingredients required for both autonomous oscillations of the internal oscillator and its response to the external driving cycle. The former aspect has received much attention, with special interest in the influence of intrinsic noise [35–37], due to the small number of molecules participating in the dynamics, and temperature variations [8,9,38–40]. In contrast, much less effort has been devoted to understanding how circadian clocks cope with fluctuations in forcing, even though daylight strongly fluctuates under natural conditions, throughout the day and from day to day. Thus, the same forcing cycle that synchronizes the clock to the Earth's rotation may also reset it erratically. Nevertheless, it has been recognized that daylight fluctuations affect entrainment accuracy [41], and recently, entrainment to natural light/dark cycles has been studied more closely [42–44]. In particular, it has been hypothesized that the need to adapt simultaneously to seasonal and weather changes has driven clock evolution towards complex architectures featuring several interlocked feedback loops [42].

Quite unexpectedly, a simple solution to this complex problem was suggested by a recent study of the circadian clock of *Ostreococcus tauri* [45]. This green unicellular alga, described as the smallest free-living eukaryote, was isolated 20 years ago from the Thau lagoon in southern France in which it is the dominant picophytoplankton [46]. This minute picoeukaryote has an extremely simple cellular organization, with only one mitochondrion and a plastid in addition to the nucleus [47]. The small genome of only 12.5 Mb is the most compact one known in a free-living eukaryote with 85% coding sequences and small intergenic regions [48]. Gene families are very much reduced, facilitating reverse genetics approaches [48–52]. *Ostreococcus* belongs to the Prasinophyceae, a group that emerged at the basis of green plants [47], and orthologs of plant-specific genes, such as the core clock players *TOC1* and *CCA1*, are found in *Ostreococcus*. For these reasons, *Ostreococcus* has emerged as a model organism for studying light and circadian clock regulations, combining functional genomics and systems biology approaches [45,49,53,54]. The importance of light/dark and circadian regulations were highlighted in a genome-wide analysis under light/dark cycles that revealed rhythmic expression for almost all genes, with strong clustering according to biological process [55]. Circadian rhythms in cell division were also observed under constant light [56]. Two orthologs of the central Arabidopsis clock genes *TOC1* and *CCA1* were identified in the *Ostreococcus* genome [49]. Functional analysis by over-expression/antisense experiments supported the hypothesis that TOC1 activates *CCA1*, whose product in turn represses *TOC1*, with biochemical evidence that CCA1 binds directly to the *TOC1* promoter. The inducible expression of *TOC1* further confirms that *TOC1* is a central clock gene in *Ostreococcus* [52]. Interestingly, these hypotheses contrast with recent re-evaluations of the role played in the Arabidopsis clock by TOC1. TOC1 had long been assumed to be an activator of *CCA1/LHY* [57–60], based on genetic data showing that reactivation of *CCA1/LHY* requires TOC1 [61]. It has recently been shown that, in Arabidopsis, TOC1 actually represses *CCA1* when binding directly to its promoter [62–64]. However, this does not preclude the possibility that TOC1 can also activate *CCA1* indirectly. In *Ostreococcus*, an activating role for TOC1 is consistent with all experimental observations, and is actually

required to ensure negative feedback along the *TOC1/CCA1* loop, as no other orthologs of the Arabidopsis clock have been identified in *Ostreococcus* [49].

The identification of *TOC1* and *CCA1* as central *Ostreococcus* clock genes led Thommen *et al.* [45] to investigate whether a simple mathematical model of the *TOC1/CCA1* transcriptional negative feedback loop described above was consistent with microarray data recorded under 12 h light/12 h dark cycles. The agreement between experimental data and a simple model based on four differential equations was excellent, providing additional support for the *TOC1/CCA1* loop hypothesis. Surprisingly, there was absolutely no indication of coupling to light in experimental data [45], as best adjustment was obtained using a free-running oscillator model. By this, we mean that there was no indication in the time series that a kinetic parameter is being modulated by the presence or absence or light, which is the primary mode of coupling between circadian clocks and the day/night cycle. This finding was later confirmed by reproducing simultaneously microarray data and translational reporter data from a different experiment using the same simple mathematical model [53].

Thommen *et al.* [45] solved this 'invisible coupling' paradox by noting that a precisely timed light-coupling mechanism may have almost no effect on the oscillator. They provided several examples of coupling schemes for which an arbitrary parameter modulation inside a specific time window induces negligible deviation from the free-running profile. Such couplings are invisible when the clock is on time, but can reset it very efficiently when the clock drifts, because coupling is then active at a time when the oscillator is responsive.

However, delicate tuning of coupling to light is not only required to shield the clock from weather fluctuations, but, perhaps more importantly, to generate varying clock signals across the year. A natural question is then whether the potentially conflicting requirements of robustness to fluctuations and flexibility in the temporal profiles generated can be reconciled and satisfied simultaneously. Is robustness achieved at the cost of flexibility, or vice versa? For example, simply phase-shifting a fixed fluctuation-resistant limit cycle throughout the year would allow the clock to track only one moment of the day.

In this paper, we consider this question by analyzing translational reporter data for the *Ostreococcus* clock genes *TOC1* and *CCA1* recorded for photoperiods varying between 2 and 22 h. Remarkably, we observed a complex variation of time profiles with photoperiod. However, we also found that all time profiles can be accurately adjusted by the simple uncoupled clock model used previously [45,53], provided we assume that the static control parameters of this model vary with photoperiod. Based on our previous work [45], these results suggest a clock that is robust to daylight fluctuations for all photoperiods.

That such a simple clock, with a clearly identified *TOC1–CCA1* one-loop central oscillator, is both robust and flexible is a fundamental and surprising result. It suggests that coupling of the *TOC1–CCA1* loop to light is under the control of a complex web of yet unidentified additional feedback loops that operate at different scales in order to tune separately the phase dynamics required for daily operation on the one hand, and the expression profile modifications required to adapt to changing conditions across the year on the other hand.

Results

Construction of the experimental target profiles

Our analysis is based on time series data for translational reporters TOC1:LUC and CCA1:LUC for the clock genes *TOC1* and *CCA1*, recorded for various light/dark sequences simulating seasonal variations in day and night length (Fig. 1). They have been obtained under the same conditions as used by Troein *et al.* in their modeling study of the *Ostreococcus* clock [54].

Cells were subjected to 24 h cycles of alternating phases of light (L) and darkness (D), hereafter termed day and night. For each cell culture, the protocol began with two cycles where the photoperiod (day length) was 12 h (0–48 h), followed by three cycles (photoperiodic cycles) with a photoperiod between 2 and 22 h (48–120 h). Two experiments were performed, hereafter referred to as 'short-day' and 'long-day' experiments (see Experimental procedures). In the first experiment, day lengths ranged from 2–12 h (Fig. 1A–F), and in the second experiment, day lengths ranged from 12–22 h (Fig. 1G–L). Eight cell cultures were exposed to the same photoperiod in the short-day experiment, and three cell cultures were exposed to the same photoperiod in the long-day experiment. The two time series with a photoperiod of 12 h (12 h light/12 h dark), i.e. one in the short-day experiment and one in the long-day experiment, have similar profiles although the timings differ slightly. This discrepancy may be due to the fact that, for experimental convenience, the long-day cell cultures experienced a phase shift of 12 h before starting the experiment. As is clearly apparent in Fig. 1, the time series corresponding to different cell cultures subjected to the same lighting sequence in a

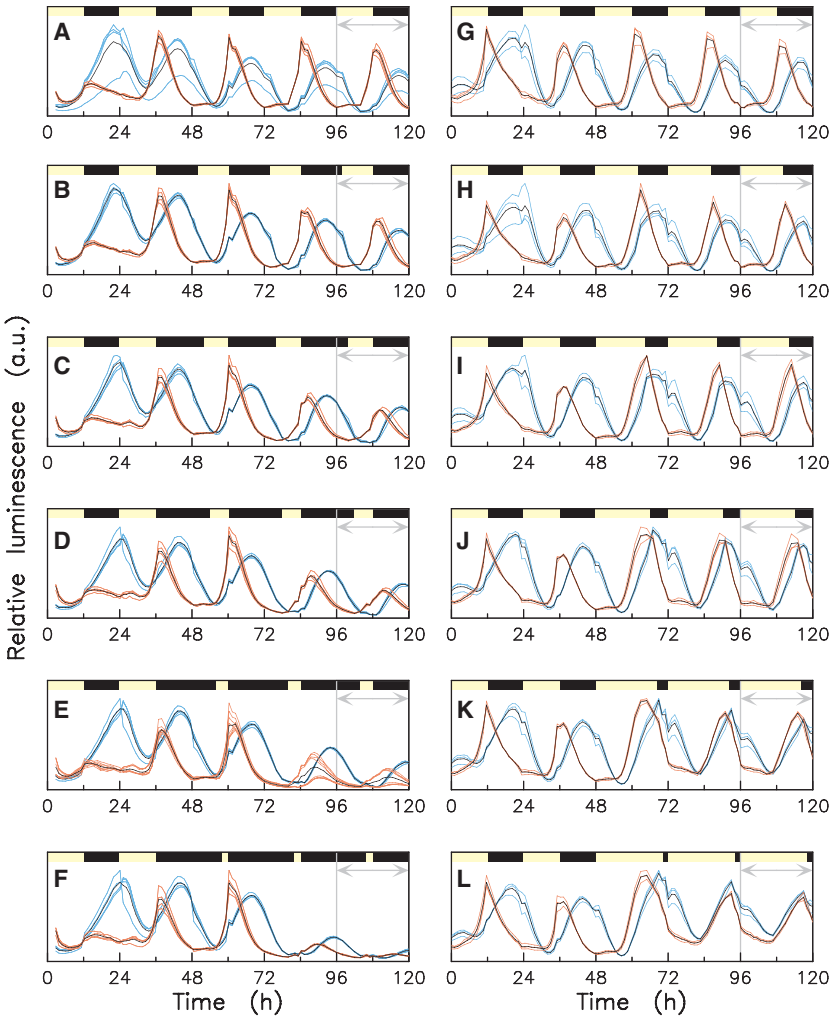

Fig. 1. Photoperiodic response of core clock components. *Ostreococcus* TOC1:LUC (red) and CCA1:LUC (blue) translational reporter lines were entrained under 24 h day/night cycles with varying day length: (A) 12 h, (B) 10 h, (C) 8 h, (D) 6 h, (E) 4 h, (F) 2 h, (G) 12 h, (H) 14 h, (I) 16 h, (J) 18 h, (K) 20 h and (L) 22 h. The yellow and black bars at the top of each panel indicate periods of light and darkness, respectively. Mean time series for translational reporter lines are indicated by black solid lines. The time interval between 96 and 120 h contains the data used for model adjustment.

given experiment are very consistent, showing the high reproducibility of the data, and enabling quantitative description of the experimental data by a mathematical model based on biochemical kinetics. The typical variation in peak timing is between 7 and 15 min for TOC1, and slightly higher for CCA1 because of the more complex profile.

Our goal is to better understand how the *Ostreococcus* clock is entrained to different cycles across the year. How do the entrained temporal profiles of the two clock genes (*TOC1* and *CCA1*), particularly their peak timings, vary with photoperiod? Is the apparent invisibility of light coupling previously observed in 12 h light/12 h dark experiments [45,53] observed for all photoperiods? Therefore, we focus here on reproducing data from the third photoperiodic cycle (between 96 and 120 h), assuming that the *Ostreococcus* clock has by then acclimated to the photoperiod change applied at time 48 h, and displays its normal response to the entrainment cycle. This 24 h interval of time is indicated by a two-headed gray arrow in Fig. 1.

The time series shown in Fig. 1 show the total luminescence emitted by a cell population. As such, they may reflect the average single-cell clock dynamics as well as variations in the total number of cells or their spatial distribution. For example, cell cultures are expected to grow faster under long days as the number

of cell division events per day was shown to increase with day length [50]. In contrast to this, the shape of the temporal expression profiles, and in particular their peak timings, provides more accurate information on the clock dynamics. To avoid capturing amplitude variations that are possibly biased by population dynamics, we normalize the data for the different photoperiods so that they have the same maximum expression level.

In order to keep the mathematical model as simple as possible and avoid over-fitting the data, we neglect the fact that luminescence is generated by reporter genes inserted into the genome in addition to the endogenous ones, and thus the over-expression of CCA1 and TOC1 induced in the respective cell lines by addition of CCA1:LUC and TOC1:LUC reporters. This over-expression may induce such effects such as variation in the free-running period. We thus use the translational reporter time series as indicators of native protein concentration, an approximation that has been assessed previously [45,53] and that is acceptable when the photon emission time is much larger than the protein degradation time. In this case, the entire CCA1:LUC or TOC1:LUC protein population, rather than the freshly synthesized proteins, contributes to luminescence. As naive as they may appear, our simplifying assumptions are justified by the fact that a more detailed model would include the simple model described below as a limiting case, and would only be useful to improve adjustment. Finally, we remove the base-level bias observed by Morant *et al.* [53] to obtain the target profiles. Indeed, comparison of luminescence signals from genetically identical cell cultures showed unambiguously the existence of a basal luminescence level at zero protein concentration.

Circadian phases of *TOC1* and *CCA1* display a complex variation with photoperiod

Before carrying out any adjustment, analysis of the target profiles revealed a complex orchestration of CCA1 and TOC1 expression by the *Ostreococcus* clock, despite its apparent simplicity. This is illustrated in Fig. 2, which shows the positions of TOC1 and CCA1 expression peaks as a function of Zeitgeber time (ZT), measured from the last dawn. Peak positions for the first and second photoperiodic cycle are also indicated, allowing estimation of the convergence to a stationary state of entrainment and providing confidence that the clock is close to the entrained state in the third photoperiodic cycle. That the rate of convergence appears lower for CCA1 peaks than for TOC1 peaks is mostly due to the more complex shape of CCA1 peaks, as the rate of convergence is a global property of the limit cycle.

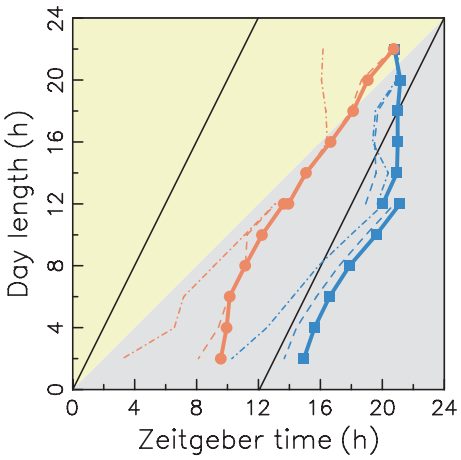

Fig. 2. Complex response of the *Ostreococcus* clock to photoperiod changes. Timings (ZT) of the concentration peaks of TOC1:LUC (red) and CCA1:LUC (blue) are shown as a function of day length. Timings for the third photoperiodic cycle (96–120 h) are shown by points connected by a thick solid line. Timings for the first and second photoperiodic cycles are indicated by dashed/dotted and dashed lines, respectively. The yellow and gray backgrounds indicate intervals of light and darkness, respectively. The solid black lines indicate the middle of the day and of the night.

Fig. 2 shows clearly that the TOC1–CCA1 oscillator does not respond to varying photoperiod by simply globally shifting its phase, but relies on a mechanism that differentially controls the peak timings of CCA1 and TOC1. The TOC1 peak tends to track dusk, except for very short days where its timing becomes roughly fixed relative to the dawn. For long days, the CCA1 peak tracks dawn, occurring at approximately ZT21, but for short days it occurs $\sim$ 1 h after the middle of the night.

The time delay between TOC1 and CCA1 expression peaks, as well as their times of occurrence in the lighting cycle, are therefore critical clock features. One objective of this study was to check whether the variations in TOC1 and CCA1 temporal profiles with photoperiod, including inter-peak delay and peak widths, can be reproduced by a mathematical model. Interestingly, it is for the pivotal case of 12 h light/12 h dark that the TOC1–CCA1 delay is larger and the expression peaks narrower (Fig. 1). As the inter-peak delay decreases, above or below a photoperiod of 12 h, expression peaks tend to broaden.

For each photoperiod, the relative position of the two expression peaks remains compatible with the hypothesis of a two-gene loop whereby TOC1 activates *CCA1* and CCA1 represses *TOC1*, except for a

photoperiod of 22 h, where the two peaks coincide. Our assumption that luminescence signals reflect true protein concentrations then reaches its limits. Over-expression of CCA1 due to insertion of *CCA1:LUC* has been shown to shorten the free-running period (FRP), whereas over-expression of TOC1 due to insertion of *TOC1:LUC* lengthens the FRP. These opposite FRP variations result in slight antagonist phase shifts of expression profiles, leading to an overlap of the expression peaks. This problem could be worked around simply by using more detailed models of the two transgenic clocks including the *CCA1:LUC* and *TOC1:LUC* genes. However, as indicated below, this is only required to improve adjustment in this particular case, encouraging us to preserve the simplicity of our model and avoid over-fitting.

Mathematical model

The minimal model of the *TOC1–CCA1* transcriptional feedback loop consists of the following four ordinary differential equations, where a dot over a variable represents its time derivative:

$$\dot{M}_{\mathrm{T}} = \mu_T + \frac{\lambda_{\mathrm{T}}}{1 + (P_{\mathrm{C}}/P_{C0})^{n_C}} - \delta_{M_{\mathrm{T}}} \frac{K_{M_{\mathrm{T}}} M_{\mathrm{T}}}{K_{M_{\mathrm{T}}} + M_{\mathrm{T}}} \quad (1a)$$

$$\dot{P}_{\mathrm{T}} = \beta_{\mathrm{T}} M_{\mathrm{T}} - \delta_{P_{\mathrm{T}}} \frac{K_{\mathrm{P_T}} P_{\mathrm{T}}}{K_{P_{\mathrm{T}}} + P_{\mathrm{T}}} \quad (1b)$$

$$\dot{M}_{\mathrm{C}} = \mu_{\mathrm{C}} + \frac{\lambda_{\mathrm{C}} (P_{\mathrm{T}}/P_{\mathrm{T0}})^{n_{\mathrm{T}}}}{1 + (\mathrm{P_T}/P_{\mathrm{T0}})^{n_{\mathrm{T}}}} - \delta_{M_{\mathrm{C}}} \frac{K_{M_{\mathrm{C}}} M_{\mathrm{C}}}{K_{M_{\mathrm{C}}} + M_{\mathrm{C}}} \quad (1c)$$

$$\dot{P}_C = \beta_{\mathrm{C}} M_{\mathrm{C}} - \delta_{P_{\mathrm{C}}} \frac{K_{P_{\mathrm{C}}} P_{\mathrm{C}}}{K_{P_{\mathrm{C}}} + P_{\mathrm{C}}} \quad (1d)$$

These equations (model 1) describe the time evolution of mRNA concentrations M_{C} and M_{T} and protein concentrations P_{C} and P_{T} for the *CCA1* and *TOC1* genes, respectively, resulting from mRNA synthesis regulated by the other protein, translation and enzymatic degradation. The *TOC1* transcription rate varies between μ_{T} at infinite CCA1 concentration and $\mu_{\mathrm{T}} + \lambda_{\mathrm{T}}$ at zero CCA1 concentration according to the usual gene regulation function with threshold P_{C0} and cooperativity n_{C}. Similarly, the *CCA1* transcription rate is μ_{C} at zero TOC1 concentration, and $\mu_{\mathrm{C}} + \lambda_{\mathrm{C}}$ at infinite TOC1 concentration, with threshold P_{T0} and cooperativity n_{T}. The TOC1 and CCA1 translation rates are β_{T} and β_{C}, respectively. For each species X, the Michaelis–Menten degradation term is written such that δ_X is the low-concentration degradation rate and K_X is the saturation threshold. Their expression is mathematically equivalent to the usual formulation using the Michaelis–Menten constant K_X and the maximum degradation speed $V_{\max} = \delta_X K_X$.

The question is often raised as to whether degradation kinetics should be described by Michaelis–Menten terms or not. It is well known that such terms favor oscillations, as do high values of the Hill coefficients in the transcriptional regulation terms [65]. Accordingly, it is commonly thought that one type of non-linearity can be used to mimic the effect of the other type, and that it is difficult to discriminate between them. We stress that such a belief does not hold true when data adjustment can be achieved with high precision, as has been possible in previous studies of the *Ostreococcus* clock [45,53] and as is the case here. Typically, parameter optimization necessarily leads to strongly saturated Michaelis–Menten kinetics whenever the decay to zero of a molecular actor follows a triangular rather than decreasing exponential shape. There is no way in which this characteristic waveform can be reproduced by tuning the Hill coefficients associated with transcriptional regulation. Such behavior has been clearly shown for *CCA1* mRNA [45], and this also the case for TOC1 protein levels (see below). The assumption of enzymatic degradation is thus perfectly justified here, all the more so as the Michaelis–Menten terms will reduce to simple linear degradation term if the data indicate.

We found previously that model 1 with no parametric modulation, corresponding to a free-running oscillator, was able to simultaneously reproduce microarray and translational reporter data recorded in two different 12 h light/12 h dark experiments, with excellent agreement [53]. To evaluate the experimental reproducibility of *Ostreococcus* clock molecular signals, we determined whether model 1 using a best-fitting parameter set obtained previously [53] could reproduce the two 12 h light/12 h dark datasets used here. As Fig. 3 shows, there is an excellent agreement with the short-day experiment recording, which is the third independent experiment reproduced by this model using this parameter set. For the long-day experiment, there is a noticeable shift in the CCA1 peak, which may result from the phase shift of 12 h experienced before the experiment, as mentioned above. However, as shown below, this does not affect our findings.

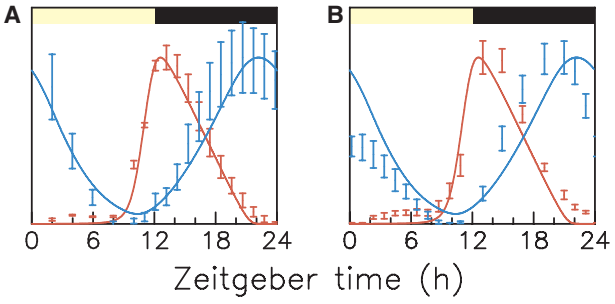

Fig. 3. Comparison of data recorded under 12 h light/12 h dark photoperiods with numerical solutions to model 1 using the parameter set obtained previously [53]. TOC1 profiles are shown in red, and CCA1 profiles are shown in blue. (A) 12 h light/12 h dark profile from the 'short-day' datasets, corresponding to signals in Fig. 1A; (B) 12 h light/12 h dark profile from the 'long-day' datasets, corresponding to signals in Fig. 1G.

Photoperiod-dependent free-running oscillator models adjust experimental data precisely

A simple way to obtain a robust coupling for all photoperiods would be to globally phase shift the robust oscillator demonstrated in previous work [45,53] depending on photoperiod, keeping the two profiles and their separation unchanged. However, the fact that the TOC1–CCA1 delay and peak widths vary significantly with photoperiod totally excludes such a possibility. It is thus quite mysterious how robustness can be achieved simultaneously for each of the profiles observed.

In order to obtain insight into how robustness combines with the flexibility observed, we tested adjustment of the expression profiles by free-running TOC1–CCA1 oscillator models whose parameters are allowed to vary with photoperiod. This amounts to performing the analysis applied to 12 h light/12 h dark datasets in our previous work separately for each photoperiod [45,53]. The parameter values of model 1 are optimized to adjust this model to the experimental profiles under the constraint that the FRP is 24 h. As discussed previously [45], this technical simplification does not imply that the actual FRP is exactly 24 h.

Figure 4A shows clearly that an impressive agreement between experimental and numerical profiles is obtained for all photoperiods. In particular, the timings of the TOC1 and CCA1 expression peaks are very well reproduced (Fig. 4B). Note the straight-line decay of the TOC1 protein level that appears clearly in several panels of Fig. 4, indicating a strongly saturated degradation and justifying the use of Michaelis–Menten degradation kinetics.

By applying the same adjustment procedure to random target profiles, we found that the probability of obtaining such a good agreement for all photoperiods by chance is exceedingly low, well below 10^{-4} (see Experimental procedures). That the *Ostreococcus* clock generates time profiles that remain so close to that of a free-running oscillator while strongly varying with photoperiod is a very important finding. As shown previously, the invisibility of coupling in entrainment conditions reflects a strategy to shield the circadian clock from daylight fluctuations [45,66]. Thus our result indicates unambiguously that robustness and flexibility can be simultaneously achieved in a simple clock built around a simple one-loop, two-gene, core oscillator. The flexibility of this oscillator is shown clearly in Fig. 4C, which shows the projections into the TOC1–CCA1 plane of the various limit cycles observed for all photoperiods.

For each photoperiod, excellent adjustment was obtained in a wide region of parameter space, a phenomenon that is often observed in systems biology models [67]. Optimal parameter sets were clustered around a single point, unlike what has been reported for a model of the mammalian clock [68], where multiple solutions were observed. Here, parameter indeterminacy indicates that the generated time profiles are very robust to parameter changes, a remarkable fact given the simplicity of the model.

When comparing parameter values corresponding to different photoperiods, there is an additional source of variation due to the fact that time series are purposely fitted up to a scaling factor both in concentrations and in time (to keep the FRP at 24 h), and that different scalings may have been used for different photoperiods. While this guarantees that only the clock dynamics are probed, possible systematic variations in expression levels with photoperiod are not captured and may manifest themselves as systematic variations in the best-fitting parameter values (see Experimental procedures).

As a result of such systematic effects combined with the robustness of fit noted above, independent adjustments for different photoperiods typically yield wildly varying parameter values. We therefore used a modified goodness of fit estimator that penalizes parameter value dispersion across photoperiods. This ensures that parameter value variations across the photoperiod range are only as large as required to reproduce the different time profiles. Figure 5 and Table 1 indicate how the obtained parameter values vary as a function of photoperiod. A number of parameters do not display a significant variation with photoperiod (e.g. λ_C, μ_T, λ_T, P_{C_0},δ_{M_T}, P_{T_0}). Moreover, the Michaelis–Menten constants K_X are such that the associated degradation mechanisms are mostly either strongly saturated

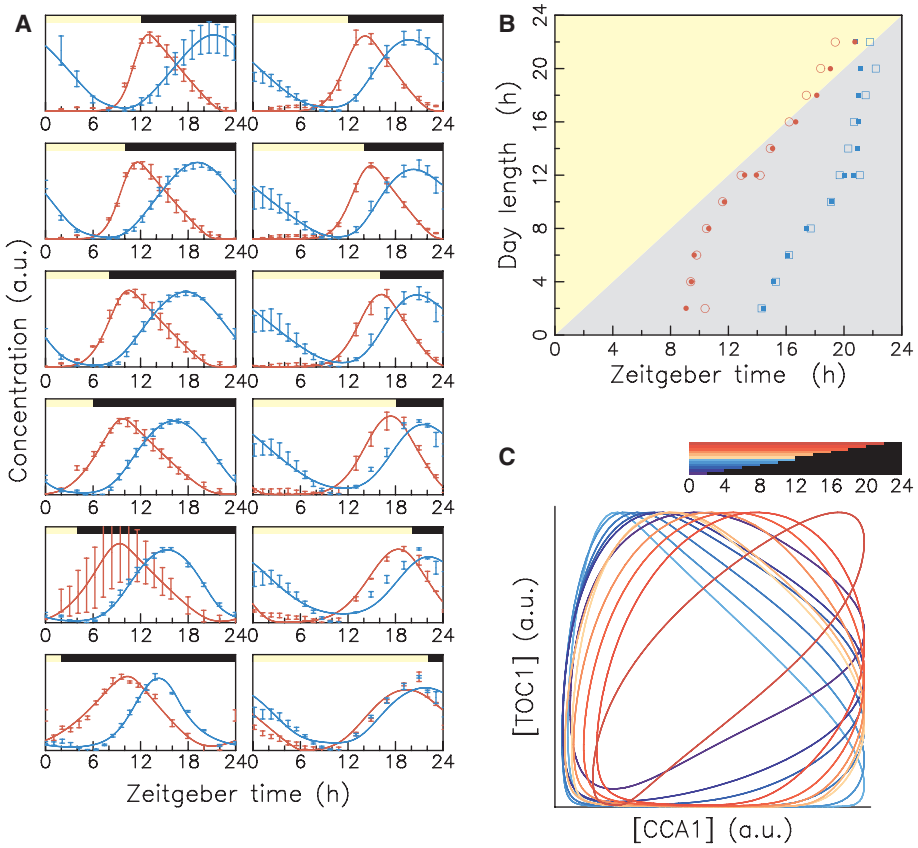

Fig. 4. Adjustment of TOC1 and CCA1 profiles by a free-running oscillator model. (A) Measured data shown in Fig. 1 are compared with numerical solutions of a free-running oscillator model (model 1) where all parameters have been adjusted for each photoperiod separately. (B) Comparison of the ZT peak timings of expression of TOC1 (red circles) and CCA1 (blue squares), for experimental data (closed symbols) and the model (open symbols). Excellent agreement was observed for both profile shapes and timings. (C) Projection of the limit cycle into the TOC1–CCA1 plane for the various photoperiods. Line color indicates photoperiod, and ranges from dark blue (2 h day length) to dark red (22 h day length); light blue and light red correspond to 12 h light/12 h dark protocols in the 'short-day' and 'long-day' experiments, respectively.

(M_C, M_T and P_T) or very far from saturation (P_C). On the other hand, translation rates appear to depend on photoperiod, with a gradual increase of β_C with photoperiod for long days and a value of β_T that is maximal for 12 h light/12 h dark and decreases for longer or shorter days. The degradation rate δ_{P_C} is notably larger for long photoperiods, even more so for the product $V_{max}P_C = \delta_{P_C}K_{P_C}$, which gives the maximal number of CCA1 proteins that can be degraded per unit time. The corresponding quantity for TOC1, $V_{max}P_T = \delta_{P_T}K_{P_T}$ also clearly depends on photoperiod, peaking for the 12 h light/12 h dark photoperiod and decreasing for longer or shorter photoperiods. Finally, the basal CCA1 transcription rate μ_C appears to be much larger for long days. Together, these observations are consistent with the idea of seasonal tuning of the TOC1–CCA1 loop using a few parameters depending on photoperiod. The parameter values for the two 12 h light/12 h dark experiments are relatively consistent between themselves as well as with the parameter values obtained previously [45].

However, at this stage, it is difficult to assess the precise biological significance of these curves because of the adjustment procedure followed. We therefore leave precise parameter estimation for a future work and concentrate here on our strategy to demonstrate how the entrained TOC1–CCA1 oscillator shows the same dynamic behavior as a free-running oscillator at all photoperiods, showing no signature of light coupling in the time series.

Robustness to daylight fluctuations in different photoperiods

In a previous paper [45], we showed how robustness to daylight fluctuations may be achieved by appropriately choosing the coupling mechanism and the coupling window timings such that the light signal does not

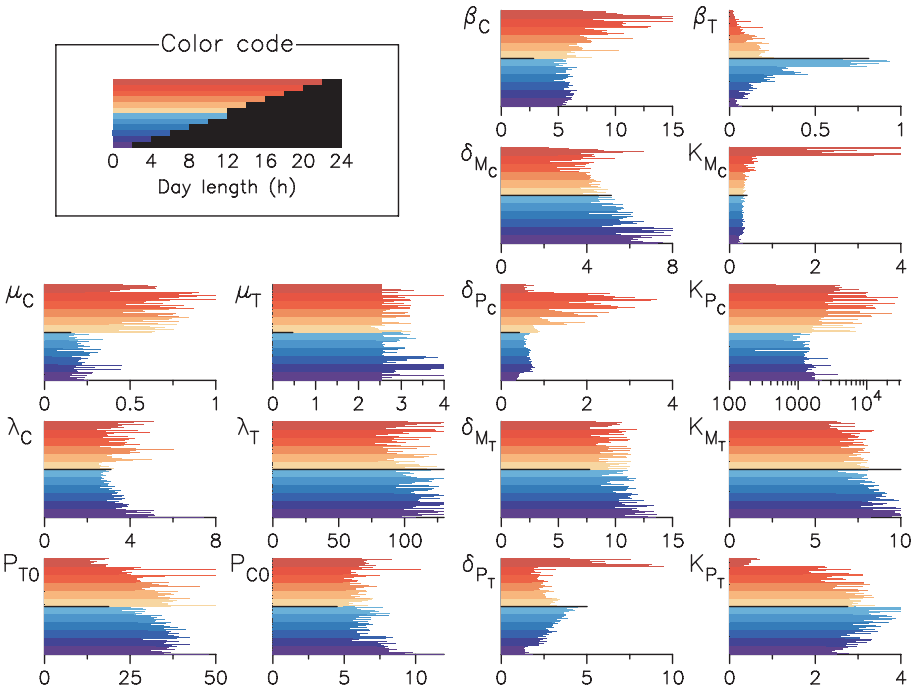

Fig. 5. Values of the best-fitting parameters used in Fig. 4 for each photoperiod. For each photoperiod, the values of the 20 best-fitting parameter sets are shown. Bar color indicates photoperiod, and ranges from dark blue (2 h day length) to dark red (22 h day length). For reference, the black line indicates the best-fit parameter value obtained in [53].

Table 1. Parameter values obtained by adjusting experimental data using a free-running model with 16 photoperiod-dependent parameters.

	Data from [53]	Short-day experiments					Long-day experiments						
Day length	12	2	4	6	8	10	12	12	14	16	18	20	22
RMS error	7.85	7.3	4.5	3.7	3.5	3.8	4.5	5.3	4.6	5.9	7.4	9.0	9.7
n_T	2	2	2	2	2	2	2	2	2	2	2	2	2
μ_C (nM·h^{-1})	0.153	0.262	0.174	0.216	0.163	0.227	0.197	0.626	0.379	0.787	0.871	0.622	0.235
λ_C (nM·h^{-1})	3.10	7.43	3.56	3.49	2.54	2.98	2.45	3.04	3.34	3.99	3.56	2.72	2.46
P_{T0} (nM)	18.7	48.1	38.8	38.5	35.4	36.8	26.8	37.0	42.6	26.3	26.6	21.8	16.2
β_C (h^{-1})	2.83	4.90	4.52	4.48	5.71	5.34	4.77	5.72	10.3	7.88	9.29	13.1	15.5
n_C	2	2	2	2	2	2	2	2	2	2	2	2	2
μ_T (nM·h^{-1})	0.467	2.54	2.82	2.50	2.58	2.59	2.96	2.54	2.54	3.20	3.20	3.22	2.92
λ_T (nM·h^{-1})	487	108	86.0	84.5	108	84.9	86.0	101	79.8	93.9	93.2	90.2	94.1
P_{C0} (nM)	4.51	14.9	8.06	7.90	6.52	5.57	7.24	4.89	6.78	5.11	4.87	4.90	6.00
β_T (h^{-1})	0.812	0.072	0.105	0.135	0.185	0.457	0.801	0.157	0.226	0.086	0.063	0.037	0.024
$1/\delta_{M_C}$ (h)	0.195	0.137	0.193	0.205	0.232	0.183	0.209	0.245	0.274	0.245	0.275	0.423	0.376
$1/\delta_{P_C}$ (h)	2.36	2.91	1.86	1.68	1.68	1.83	2.08	1.16	0.654	0.444	0.370	0.286	1.79
$1/\delta_{M_T}$ (h)	0.129	0.074	0.097	0.098	0.103	0.114	0.119	0.106	0.107	0.115	0.120	0.125	0.122
$1/\delta_{P_T}$ (h)	0.199	0.538	0.644	0.630	0.400	0.318	0.273	0.394	0.339	0.533	0.563	0.479	0.105
K_{M_C} (nM)	0.407	0.303	0.250	0.250	0.268	0.274	0.273	0.345	0.303	0.407	0.463	0.559	3.364
K_{P_C} (nM)	75.9	2237	1386	1258	1168	1105	843	1579	2239	12054	13648	14678	10575
K_{M_T} (nM)	28.3	8.25	8.17	8.09	9.21	6.70	7.72	6.68	6.65	7.22	6.93	7.51	5.70
K_{P_T} (nM)	2.76	2.50	2.98	3.04	2.99	3.71	3.31	2.91	2.79	3.24	3.12	1.70	0.273

perturb the dynamics of the entrained core oscillator, which thus appears to be free-running. However, window timings depend crucially on the limit-cycle shape. In the sections above, we have shown that the limit cycle of the TOC1–CCA1 core oscillator is significantly deformed as photoperiod is varied, but that the

invisibility of coupling persists in all cases. Thus it is important to show how robustness to daylight fluctuations may be ensured in all seasons by adjusting coupling windows adequately. This will also allow us to determine the essential dynamic ingredients of this robustness.

For definiteness, we assume an hypothetical coupling where the core TOC1–CCA1 oscillator is driven by the day/night cycle via transient modulation of parameter δ_{P_T} (TOC1 degradation rate). Other molecular interactions can lead to robust couplings [45], but the analysis is similar in each case. For the sake of simplicity, this modulation is assumed to occur in a temporal window that is fixed relative to the day/night cycle. There is no loss of generality if we only intend to understand the behavior in entrainment, not the dynamics of resetting after a large phase excursion. How such a parametric forcing ensures a stable phase relationship between the clock and the day/night cycle, while shielding the clock from daylight fluctuations, can be understood as follows.

The action of a parametric modulation on an oscillator is described by the impulse phase response curve (iPRC) [8,43,66], which is somewhat similar to the notion of a circadian integrated response characteristic recently proposed by Roenneberg *et al.* [69,70]. The iPRC gives the phase shift induced by an infinitesimal parameter perturbation with unit time integral as a function of the position along the limit cycle. Figure 6A shows the iPRCs of the TOC1 degradation modulation computed for the entrained limit cycles observed at varying photoperiods. Although the shape of these iPRCs slightly varies for the distinct limit cycles, it is remarkable that the flat part of the iPRC persists. This conserved feature of the iPRC, also known as a dead zone, reflects the insensitivity of the limit cycle to TOC1 degradation modulation over the time period where TOC1 protein levels are low, in particular at the start of the day. This implies that the coupling profile can be designed to match these intervals of insensitivity, allowing the clock to be robustly entrained by fluctuating forcing [66]. When the clock is on time, the coupling window and the dead zone coincide, preventing fluctuations from disrupting the clock. Clock drifting destroys the coincidence, allowing coupling to reset the clock as needed.

Note that, in the limit of weak coupling, the total phase shift $\delta\varphi$ induced by the parameter perturbation profile $\delta p(t)$ is given by $\delta\varphi = \int_{t_{on}}^{t_{off}} Z(t)\delta p(t)\mathrm{d}t$ where $Z(t)$ is the iPRC and t_{on} and t_{off} are the start and end

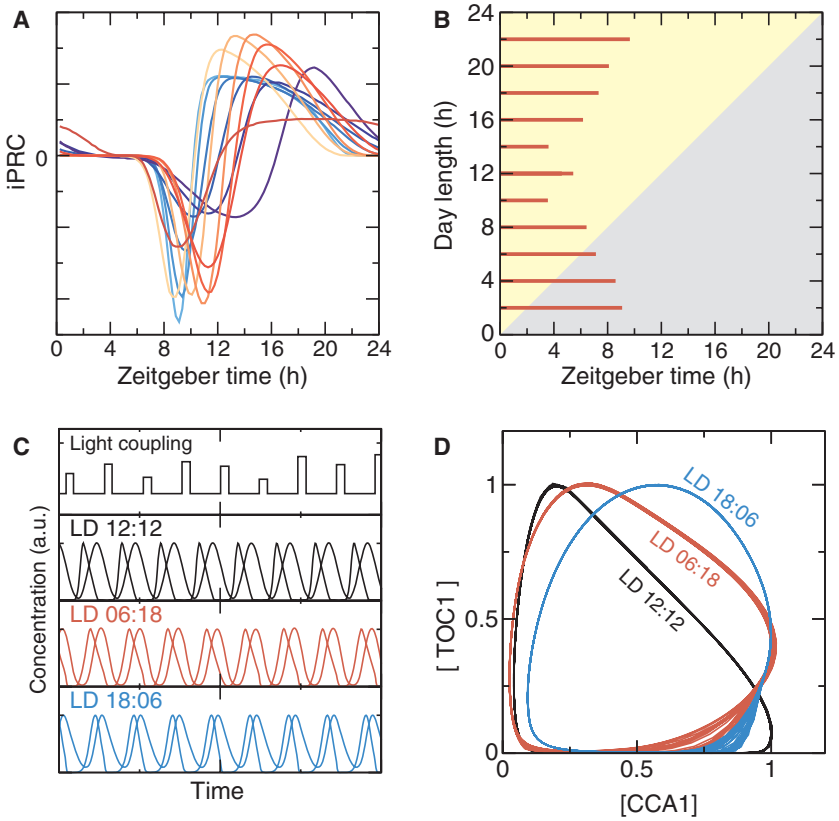

Fig. 6. Robust coupling to light at different photoperiods. (A) Phase response curves (iPRCs) of the various photoperiod-dependent free-running oscillators in response to an impulse perturbation of the TOC1 degradation rate. (B) Robust coupling windows in which the TOC1 degradation rate is multiplied by two and that begin at ZT0 such that adjustment of the model to experimental data is preserved (no deformation of the limit cycle). (C) For three different photoperiods (12 h light/12 h dark, 6 h light/18 h dark and 18 h light/6 h dark), entrained TOC1/CCA1 oscillatory profiles are insensitive to fluctuations of TOC1 degradation rates (modulation factor uniformly distributed between 1 and 3) inside the coupling windows in (B). (D) Limit cycles corresponding to the profiles shown in (C), showing the small residual fluctuations.

of the coupling window. For an FRP of ~ 24 h, stationary operation requires a $\delta\varphi$ of approximately zero, so the coupling window $[t_{on}, t_{off}]$ must be located around a zero of the iPRC $Z(t)$. A stable operation also requires a negative derivate of $Z(t)$ at this zero.

For each photoperiod, we searched for coupling windows inside which TOC1 degradation can be increased without affecting model adjustment compared to the uncoupled model. This is a stronger requirement than the zero phase shift condition as it also implies that deviation from the limit cycle is minimal. Figure 6B shows the localizations of such windows, where for definiteness coupling activation was fixed at ZT0 and the increase of the TOC1 degradation rate during the coupling window was 100%. In fact, the window timings almost did not depend on the modulation factor chosen, indicating that the same limit cycle, close to the uncoupled one, is obtained at different coupling strengths, and hence light levels. Interestingly, window timings are relatively symmetrical between the short and long photoperiods.

As Fig. 6C shows, this insensitivity of the adjustment with respect to modulation strength ensures that the circadian oscillator is robust to daylight fluctuations. We subjected the limit cycles obtained for three different photoperiods (12 h light/12 h dark, 6 h light/18 h dark and 18 h light/6 h dark) to a random sequence of modulation depths. On each day, the TOC1 degradation rate inside the coupling window shown in Fig. 6B was multiplied by a random factor uniformly distributed between 1 and 3. This describes adequately the effect of daylight variations from one day to the next, which are the most disruptive because they are resonant with the oscillator [45]. It can be seen that the circadian clock ticks very robustly in the three cases, delivering signals that are almost identical to those of a free-running oscillator even though strong coupling operates for several hours (Fig. 6B). Obviously, this only holds when the oscillator has the phase observed experimentally. Otherwise, the zero phase shift condition is not satisfied and the coupling rapidly resets the clock to the correct time.

Figure 6D shows the three limit cycles under random forcing, showing small residual fluctuations. Interestingly, these are stronger for the two extreme photoperiods than for the 12 h light/12 h dark protocol, which is impressively insensitive to fluctuations. Figure 6D, with its clearly distinct limit cycles, illustrates nicely how robustness to daylight fluctuations and flexibility can be combined in a simple clock provided coupling to light is suitably designed. To summarize, adjustment of circadian signals by a free-running oscillator model does not imply that there is no coupling, but rather that coupling is scheduled such that it does not affect the oscillator when the clock is entrained, thereby shielding it from daylight fluctuations.

Discussion and Conclusion

In this paper, we have studied the response of the *Ostreococcus* circadian clock to day/night cycles of various day lengths such as those induced by seasonal changes. Analysis of the photoperiod-dependent expression profiles of the two central clock proteins TOC1 and CCA1 allowed us to reveal two remarkable features of the *Ostreococcus* clock photoperiodic behavior.

First, a flexible and complex variation of circadian output profiles with photoperiod is observed, reminiscent of that observed in the higher plant Arabidopsis [24] or in *Neurospora crassa* [25,26]. Not only is there a complex response of the oscillator phase to varying photoperiod [26,54], but the time interval between the two expression peaks and the waveform of the profiles also change significantly with photoperiod. More precisely, TOC1 expression tends to follow the day/night transition, except in shorter days where it remains fixed relative to dawn, whereas CCA1 expression is scheduled in the middle of the night, except for longer days where it tracks dawn (Fig. 2). Therefore, at least two phases rather than a single one are needed to describe entrainment of the *Ostreococcus* clock to different photoperiods. More generally, the variation of timings with photoperiod is consistent with the view that a circadian clock must deliver different signals in different seasonal contexts because different physiological processes must be controlled at different times of the day. This was confirmed experimentally by a transcriptomic genome-wide survey that revealed temporal clusters of genes involved in specific biological processes such as DNA replication, mitosis, translation, photosynthesis or lipid metabolism in *Ostreococcus* cells exposed to day/night cycles [55].

Second, we found that protein expression data for all photoperiods can be adjusted with surprising accuracy by a minimal model of the TOC1–CCA1 transcriptional loop with no forcing by light, provided that its kinetic parameters are allowed to vary with photoperiod to account for the flexible response observed. We showed that the probability of such behavior being observed for random profiles is extremely low.

This remarkable finding not only confirms the central role of the TOC1–CCA1 loop in the *Ostreococcus* circadian clock [45,53,54,71], but also provides further evidence that, when entrained, this clock becomes 'blind' to the light-coupling mechanisms that synchronize it to the day/night cycle. As shown previously,

this behavior is easily explained if activation of the light input pathway coincides with a 'dead zone' of the phase response curve of the circadian oscillator [45,66]. This simple design ensures that the clock generates the same profiles under very different daylight intensities, which makes it naturally insensitive to fluctuating forcing. That such behavior is observed at all photoperiods, for very different limit-cycle geometries, suggests that the molecular signals of the *Ostreococcus* clock have been strongly shaped by the requirement to be robust to daylight fluctuations in all seasons. This evolutionary constraint is all the stronger in *Ostreococcus* as the light perceived by this marine organism varies not only due to sky cover but also depending on the distance to the water surface and the water turbidity.

Flexibility and robust synchronization to the day/night cycle both rely on the architecture of the light input pathways and feedback loops interacting with the TOC1–CCA1 oscillator, about which little is currently known despite recent progress [52,72]. Together, our results suggest that there is a clear distinction of light-coupling processes according to dynamic role and time scale.

On one hand, gated coupling mechanisms, whereby a kinetic parameter is modulated for a few hours, are required to ensure entrainment and keep the oscillation phase stable from day do day. Gated light inputs are a feature of many circadian clocks, and it has been proposed that they are critical for generating appropriate timings under different photoperiods [31]. Closely related phenomena are light adaptation or response saturation [43,73,74]. As discussed above, the fast inputs synchronizing a robust clock to the day/night cycle must be tuned so that they do not deform the entrained limit cycle, which would otherwise be exposed to daylight fluctuations [45]. But how can we explain the slow annual changes in the limit cycle required to adapt clock signals to different seasons? Our findings suggest that the flexible variation of expression profiles with photoperiod relies on slow inputs modifying kinetic parameters of the core oscillator over a time scale of several days. Indeed, the existence of such slow kinetic changes naturally explains why the variation of expression profiles with photoperiod is perfectly matched by a free-running oscillator model with photoperiod-dependent parameters. Such slow changes may be related to light accumulation processes, coincidence mechanisms or metabolism, and more generally to the presence of molecular actors that are constitutively expressed at photoperiod-dependent levels. In fact, this separation in fast mechanisms maintaining phase and slow mechanisms controlling expression profiles is only a necessary condition for robustness, as the synchronizing couplings and their phase response curves must also satisfy specific constraints to ensure a reproducible phase dynamics over a wide range of operating conditions [66].

Interpretation of our results probably requires clarification as to how our modeling strategy differs from conventional approaches. In order to reveal the design principles underlying the interplay of robustness and flexibility, we have purposely used an incomplete model that describes the internal dynamics of the TOC1–CCA1 core oscillator but does not include the actors influencing its behavior. More precisely, we have not specified the external actors or feedback loops that transiently modulate the TOC1–CCA1 loop to synchronize it to the day/night cycle and fix the phase of its oscillations, nor those that affect its kinetic parameters over longer time scales to adjust the limit cycle as needed. This strategy is of course only possible because the dynamics of the TOC1–CCA1 loop appear to be largely autonomous by design. Its benefit lies in the fact that if we had incorrectly hypothesized the structure of light inputs, the remarkable properties revealed in this work would have been completely masked.

A direction for future work is to implement the design principles identified here in a detailed mechanistic model of the *Ostreococcus* clock, which is not an easy task. For example, an important open question is the minimal number of fast and slow inputs required to reproduce the variations of entrainment phases and expression profiles with photoperiod. In this respect, it would be interesting to analyze the *Ostreococcus* clock model proposed by Troein *et al.* [54] in the light of our results. This model, which takes into account the detailed dynamics of the luminescent reporters, was constructed from an extensive dataset obtained under the same experimental conditions as our time series. Both limit-cycle profiles and transient behavior (change in photoperiod, transition into constant light) were taken into account to adjust the mathematical model. Troein *et al.* concluded that the complex behavior of the one-loop *Ostreococcus* clock may be explained by the presence of five different light inputs into CCA1–TOC1 loop, seemingly contradicting our results. It may be that these light inputs are gated by the profiles of the actors they affect. Interestingly, the profiles generated by this model were relatively smooth, except at dawn and dusk, which could indicate weak effective coupling. The light accumulator present in this model is similar to a slow input, although it appears to be operating on a time scale that is too short to ensure robustness,

and probably cannot reproduce alone the flexibility observed in expression profiles.

It would also be interesting to compare our results to those obtained in a previous study [24] in which the flexibility of increasingly complex models of the Arabidopsis clock was studied and compared to experimental results. It was shown that mechanistic models of this circadian clock require at least three feedback loops to generate timing patterns that are not limited to tracking dawn or dusk and that reproduce those observed experimentally. This finding is consistent with the theoretical prediction that flexibility requires several interlocked feedback loops [8,9,75]. However, our results seem to imply that a clock architecture based around a single loop with photoperiod-dependent parameters is able to generate very complex patterns, whereby, for example, CCA1 can track dawn or the middle of the night depending on photoperiod. This contradiction may be apparent only, as the light inputs synchronizing the clock phases or shaping the limit cycle may belong to additional feedback loops that remain to be discovered. The invisibility of these loops under entrainment conditions certainly complicates their identification, which will require analysis of transient behavior in resetting experiments. In any case, our findings suggest that more attention should be paid to the role of slow light inputs, serving as photoperiod sensors. Such slow effects of light have recently been demonstrated in mice [76].

Clearly, the *Ostreococcus* clock has not yet revealed all its secrets. Our partial results suggest that unraveling them may reveal important design principles in circadian biology, due to the surprising agreement between mathematical models and experimental data that can be obtained in this model organism. Whatever molecular model of the *Ostreococcus* clock eventually emerges, an important lesson from the *Ostreococcus* clock response to photoperiod changes will undoubtedly be that even a simple circadian clock can combine robust and flexible mechanisms to adapt to changing weather and seasons. Another challenge will be to determine how the simple *TOC1–CCA1* transcriptional feedback loop that lies at the core of the clock interacts with the post-transcriptional clock recently demonstrated to sustain circadian rhythms under various environmental conditions in *Ostreococcus* [77].

Experimental procedures

Experimental data

The experimental data were obtained as described by Corellou *et al.* [49] under the same experimental conditions as used by Troein *et al.* [54]. They were acquired in two separate experiments, referred to as 'short-day' and 'long-day' experiments. In each experiment, part of the plate carrying cell cultures was covered by a screen that was displaced every other hour to expose different populations to different photoperiods. For experimental convenience, the 'long-day' cell cultures were exposed to a phase shift of 12 h before starting recording, so that both light-on and light-off transitions occur during working hours.

We did not use the transcriptional reporter data available. Indeed, Djouani-Tahri *et al.* [72] showed directly, using inhibitors of translation, that the time between luciferase synthesis and photon emission is extremely long, with a half-life of 5–6 h. This is the time required to observe a significant decrease in luminescence when translation is blocked. A conclusion of our previous studies [45,53] is that the transcriptional activities of both *TOC1* and *CCA1* are confined to much shorter time interval. As a result, the signal of interest, namely transcriptional activity, is probably blurred in the transcriptional reporter luminescence data, which may destabilize the adjustment procedure.

Target profiles

The target profiles of protein concentration were obtained from the luminescence records of the translational reporter lines during the third photoperiodic cycle (from 96–120 h in Fig. 1). Luminescence time series display variations in amplitude from day to day due to fluctuations in the number of cells contributing to light emission and other unknown factors. To correct this effect approximately and obtain periodic target profiles, the time series were divided by a first-order polynomial function of time interpolating between the luminescence intensities at 96 and 120 h. The base level was then removed from the time series to correct for the bias observed previously [53], and periodic profiles for all photoperiods were then re-scaled to the same maximum value.

Adjustment and goodness of fit

Model 1 includes 16 free continuously varying parameters in addition to the cooperativities n_C and n_T that are set to integer values of 2. Two solutions of model 1 that have the same waveform but different amplitudes are considered equivalent. Although this allows us to factor out population effects, it makes it more complicated to compare parameter sets resulting from optimization, because each is actually the representative of a four-dimensional manifold of equivalent points in parameter space. This is adequate for our purposes as our goal here is to establish the relevance of the free-running TOC1–CCA1 oscillator model for all photoperiods, not to estimate accurate parameter values. To measure the goodness of fit for a given parameter set,

the two numerical protein profiles are re-scaled to have the same maximum value as the experimental profiles, and compared with the latter by calculating the root mean square (RMS) error.

The parameter values reported in Fig. 5 and Table 1 are re-scaled so that the protein profiles have a maximal value of 100 nM and the mRNA profiles have maximal values in the same proportion as in microarray data recorded with a 12 h day length, i.e. 10 nM for *CCA1* mRNA and 72 nM for *TOC1* mRNA. This makes it easier to compare regulation thresholds and degradation saturation thresholds relative to the maximum values of the four concentrations, regardless of the photoperiod.

Optimization

Adjustment was performed using a population-based meta-heuristic method (harmony search [78]) for the initial large-scale search, followed by a non-linear optimization procedure based on a modified Levenberg–Marquardt algorithm (MINPACK software suite [79]) to refine the optimal parameter values. The procedure constrains the FRP at a value of 24 h, and the goodness of fit includes both the RMS error and a penalty proportional to the Eulerian distance between the current parameter set and the reference one [53]. This penalty maximizes correlation between the various best-fitting parameter sets and makes their comparison easier. Numerical integration of ordinary differential equations was performed using the SEULEX algorithm [80]. The exhaustivity of the harmony search stage and the convergence of the adjustment were monitored by checking that the optimum was reached repeatedly.

Probability of adjustment by free-running oscillators

In order to show that simultaneous adjustment of photoperiodic data by free-running oscillators is biologically significant, it is important to show that such a numerical result cannot be obtained by chance. We therefore generated a large number of random target profiles that were fed to the optimization procedure. The random protein profiles (one for TOC1 and one for CCA1) featured a single peak per period, obtained by interpolating three control points with a cubic spline. A TOC1–CCA1 delay was then chosen at random between 2 and 12 h. This yields smoothly varying profiles similar to the experimental ones and to those generated by a free-running model comprising four ordinary differential equations.

We found that, for this set of random profiles, the probability of obtaining a RMS error as good as obtained in Fig. 4 is always lower than 0.4. The upper bound of the probability of obtaining 11 (one for each photoperiod) such adjustments is thus 4×10^{-5}.

Acknowledgement

This work was supported by the Ministry of Higher Education and Research, the Nord-Pas de Calais Regional Council and Fonds Européen de Développement Economique des Régions through the Contrat de Projets État-Région (CPER) 2007–2013.

References

1 Alon U (2006) *An Introduction to Systems Biology: Design Principles of Biological Circuits*. Chapman Hall/CRC, New York.
2 Savageau M (2001) Design principles for elementary gene circuits: elements, methods, and examples. *Chaos* **11**, 142–159.
3 Novak B & Tyson J (2008) Design principles of biochemical oscillators. *Nat Rev Mol Cell Biol* **9**, 981–991.
4 Hartwell L, Hopfield J, Leibler S & Murray A (1999) From molecular to modular cell biology. *Nature* **402**, C47–C52.
5 Mengel B, Hunziker A, Pedersen L, Trusina A, Jensen MH & Krishna S (2010) Modeling oscillatory control in NF-κB, p53 and Wnt signaling. *Curr Opin Genet Dev* **20**, 656–664.
6 Kobayashi T & Kageyama R (2009) Dynamic advances in NF-κB signaling analysis. *Sci Signal* **2**, 47.
7 Alon U (2003) Biological networks: the tinkerer as an engineer. *Science* **301**, 1866–1867.
8 Rand DA, Shulgin BV, Salazar D & Millar AJ (2004) Design principles underlying circadian clocks. *J R Soc Interface* **1**, 119–130.
9 Rand D (2008) Mapping global sensitivity of cellular network dynamics: sensitivity heat maps and a global summation law. *J R Soc Interface* **5**, S59–S69.
10 Stelling J, Sauer U, Szallasi Z, Doyle F & Doyle J (2004) Robustness of cellular functions. *Cell* **118**, 675–685.
11 Kollmann M, Lovdok L, Bartholome K, Timmer J & Sourjik V (2005) Design principles of a bacterial signalling network. *Nature* **438**, 504–507.
12 Ukai H & Ueda HR (2010) Systems biology of mammalian circadian clocks. *Annu Rev Physiol* **72**, 579–603.
13 Yamada YR & Forger DB (2010) Multiscale complexity in the mammalian circadian clock. *Curr Opin Genet Dev* **20**, 626–633.
14 Roenneberg T, Chua EJ, Bernardo R & Mendoza E (2008) Modelling biological rhythms. *Curr Biol* **18**, R826–R835.
15 Dunlap JC (1999) Molecular bases for circadian clocks. *Cell* **96**, 271–290.
16 Young MW & Kay S (2001) Time zones: a comparative genetics of circadian clocks. *Nat Genet* **2**, 702–715.
17 Nuesslein-Hildesheim B, O'Brien J, Ebling F, Maywood E & Hastings M (2000) The circadian cycle of mPER clock gene products in the suprachiasmatic nucleus of

the Siberian hamster encodes both daily and seasonal time. *Eur J Neurosci* **12**, 2856–2864.
18 Tan Y, Merrow M & Roenneberg T (2004) Photoperiodism in *Neurospora crassa*. *J Biol Rhythms* **19**, 135–143.
19 Tauber E & Kyriacou B (2001) Insect photoperiodism and circadian clocks: models and mechanisms. *J Biol Rhythms* **16**, 381–390.
20 Imaizumi T & Kay SA (2006) Photoperiodic control of flowering: not only by coincidence. *Trends Plant Sci* **11**, 550–558.
21 Salazar JD, Saithong T, Brown PE, Foreman J, Locke JCW, Halliday KJ, Carr IA, Rand DA & Millar AJ (2009) Prediction of photoperiodic regulators from quantitative gene circuit models. *Cell* **139**, 1170–1179.
22 Bradshaw W & Holzapfel C (2010) What season is it anyway? circadian tracking vs. photoperiodic anticipation in insects. *J Biol Rhythms* **25**, 155–165.
23 Meijer J, Michel S, Vanderleest H & Rohling J (2010) Daily and seasonal adaptation of the circadian clock requires plasticity of the SCN neuronal network. *Eur J Neurosci* **32**, 2143–2151.
24 Edwards KD, Akman OE, Knox K, Lumsden PJ, Thomson AW, Brown PE, Pokhilko A, Kozma-Bognar L, Nagy F, Rand DA *et al.* (2010) Quantitative analysis of regulatory flexibility under changing environmental conditions. *Mol Syst Biol* **6**, 424.
25 Akman O, Rand D, Brown P & Millar A (2010) Robustness from flexibility in the fungal circadian clock. *BMC Syst Biol* **4**, 88.
26 Remi J, Merrow M & Roenneberg T (2010) A circadian surface of entrainment: varying T, τ, and photoperiod in *Neurospora crassa*. *J Biol Rhythms* **25**, 318–328.
27 Koh K, Zheng X & Sehgal A (2006) JETLAG resets the *Drosophila* circadian clock by promoting light-induced degradation of TIMELESS. *Science* **312**, 1809–1812.
28 Leloup J & Goldbeter A (1998) A model for circadian rhythms in *Drosophila* incorporating the formation of a complex between the PER and TIM proteins. *J Biol Rhythms* **13**, 70–87.
29 Mas P, Kim W, Somers D & Kay S (2003) Targeted degradation of TOC1 by ZTL modulates circadian function in *Arabidopsis thaliana*. *Nature* **426**, 567–570.
30 Johnson C, Elliott J & Foster R (2003) Entrainment of circadian programs. *Chronobiol Int* **20**, 741–774.
31 Geier F, Becker-Weimann S, Kramer A & Herzel H (2005) Entrainment in a model of the mammalian circadian oscillator. *J Biol Rhythms* **20**, 83–93.
32 Bagheri N, Taylor SR, Meeker K, Petzold LR & Doyle FJ (2008) Synchrony and entrainment properties of robust circadian oscillators. *J R Soc Interface* **5**, S17–S28.
33 Mondragon-Palomino O, Danino T, Selimkhanov J, Tsimring L & Hasty J (2011) Entrainment of a population of synthetic genetic oscillators. *Science* **333**, 1315–1319.
34 Abraham U, Granada AE, Westermark PO, Heine M, Kramer A & Herzel H (2010) Coupling governs entrainment range of circadian clocks. *Mol Syst Biol* **6**, 438.
35 Barkai N & Leibler S (2000) Biological rhythms: circadian clocks limited by noise. *Nature* **403**, 267–268.
36 Gonze D, Halloy J & Goldbeter A (2002) Robustness of circadian rhythms with respect to molecular noise. *Proc Natl Acad Sci USA* **99**, 673–678.
37 Zwicker D, Lubensky DK & ten Wolde PR (2010) Robust circadian clocks from coupled protein-modification and transcription–translation cycles. *Proc Natl Acad Sci USA* **107**, 22540–22545.
38 Pittendrigh CS (1954) On temperature independence in the clock system controlling emergence time in Drosophila. *Proc Natl Acad Sci USA* **40**, 1018–1029.
39 Rensing L & Ruoff P (2002) Temperature effect on entrainment, phase shifting, and amplitude of circadian clocks and its molecular bases. *Chronobiol Int* **19**, 807–864.
40 Brettschneider C, Rose R, Hertel S, Axmann I, Heck A & Kollmann M (2010) A sequestration feedback determines dynamics and temperature entrainment of the KaiABC circadian clock. *Mol Syst Biol* **6**, 389.
41 Beersma DGM, Daan S & Hut RA (1999) Accuracy of circadian entrainment under fluctuating light conditions: contributions of phase and period responses. *J Biol Rhythms* **14**, 320–329.
42 Troein C, Locke JCW, Turner MS & Millar AJ (2009) Weather and seasons together demand complex biological clocks. *Curr Biol* **19**, 1961–1964.
43 Taylor SR, Webb AB, Smith KS, Petzold LR & Doyle FJ (2010) Velocity response curves support the role of continuous entrainment in circadian clocks. *J Biol Rhythms* **25**, 138–149.
44 Domijan M & Rand DA (2011) Balance equations can buffer noisy and sustained environmental perturbations of circadian clocks. *Interface Focus* **1**, 177–186.
45 Thommen Q, Pfeuty B, Morant P, Corellou F, Bouget F & Lefranc M (2010) Robustness of circadian clock to daylight fluctuations: hints from the picoeucaryote *Ostreococcus tauri*. *PLoS Comput Biol* **6**, e1000990.
46 Courties C, Vaquer A, Troussellier M, Lautier J, Chretiennot-Dinet MJ, Neveux J, Machado MC & Claustre H (1994) Smallest eukaryotic organism. *Nature* **370**, 255.
47 Chretiennot-Dinet MJ, Courties C, Vaquer A, Neveux J, Claustre H, Lautier J & Machado MC (1995) A new marine picoeukaryote: *Ostreococcus tauri* gen. et sp. nov. (chlorophyta, prasinophyceae). *Phycologia* **4**, 285–292.
48 Derelle E, Ferraz C, Rombauts S, Rouz P, Worden AZ, Robbens S, Partensky F, Degroeve S, Echeyni S, Cooke R *et al.* (2006) Genome analysis of the smallest free-living

eukaryote *Ostreococcus tauri* unveils many unique features. *Proc Nat Acad Sci USA* **103**, 11647–11652.
49 Corellou F, Schwartz C, Motta J-P, Djouani-Tahri EB, Sanchez F & Bouget F-Y (2009) Clocks in the green lineage: comparative functional analysis of the circadian architecture in the picoeukaryote *Ostreococcus*. *Plant Cell* **21**, 3436–3449.
50 Moulager M, Corellou F, Verge V, Escande M-L & Bouget F-Y (2010) Integration of light signals by the retinoblastoma pathway in the control of S phase entry in the picophytoplanktonic cell *Ostreococcus*. *PLoS Genet* **6**, e1000957.
51 Heijde M, Zabulon G, Corellou F, Ishikawa T, Brazard J, Usman A, Sanchez F, Plaza P, Martin M, Falciatore A *et al*. (2010) Characterization of two members of the cryptochrome/photolyase family from *Ostreococcus tauri* provides insights into the origin and evolution of cryptochromes. *Plant, Cell Environ* **33**, 1614–1626.
52 Djouani-Tahri E-B, Christie JM, Sanchez-Ferandin S, Sanchez F, Bouget F-Y & Corellou F (2011) A eukaryotic LOV-histidine kinase with circadian clock function in the picoalga *Ostreococcus*. *Plant J* **65**, 578–588.
53 Morant P-E, Thommen Q, Pfeuty B, Vandermoere C, Corellou F, Bouget F-Y & Lefranc M (2010) A robust two-gene oscillator at the core of *Ostreococcus tauri* circadian clock. *Chaos* **20**, 045108.
54 Troein C, Corellou F, Dixon LE, van Ooijen G, ONeill JS, Bouget F-Y & Millar AJ (2011) Multiple light inputs to a simple clock circuit allow complex biological rhythms. *Plant J* **66**, 375–385.
55 Monnier A, Liverani S, Bouvet R, Jesson B, Smith JQ, Mosser J, Corellou F & Bouget F-Y (2010) Orchestrated transcription of biological processes in the marine picoeukaryote *Ostreococcus* exposed to light/dark cycles. *BMC Genomics* **11**, 192.
56 Moulager M, Monnier A, Jesson B, Bouvet R, Mosser J, Schwartz C, Garnier L, Corellou F & Bouget F-Y (2007) Light-dependent regulation of cell division in *Ostreococcus*: evidence for a major transcriptional input. *Plant Physiol* **144**, 1360–1369.
57 Locke JCW, Millar AJ & Turner MS (2005) Modelling genetic networks with noisy and varied experimental data: the circadian clock in *Arabidopsis thaliana*. *J Theor Biol* **234**, 383–393.
58 Locke JCW, Southern MM, Kozma-Bognr L, Hibberd V, Brown PE, Turner MS & Millar AJ (2005) Extension of a genetic network model by iterative experimentation and mathematical analysis. *Mol Syst Biol* **1**, 2005.0013, doi:10.1038/msb4100018.
59 Locke JCW, Kozma-Bognar L, Gould PD, Feher B, Kevei E, Nagy F, Turner MS, Hall A & Millar AJ (2006) Experimental validation of a predicted feedback loop in the multi-oscillator clock of *Arabidopsis thaliana*. *Mol Syst Biol* **2**, 59.
60 Pokhilko A, Hodge SK, Stratford K, Knox K, Edwards KD, Thomson AW, Mizuno T & Millar AJ (2010) Data assimilation constrains new connections and components in a complex, eukaryotic circadian clock model. *Mol Syst Biol* **6**, 416.
61 Alabadi D, Oyama T, Yanovsky MJ, Harmon FG, Mas P & Kay SA (2001) Reciprocal regulation between TOC1 and LHY/CCA1 within the Arabidopsis circadian clock. *Science* **293**, 880–883.
62 Gendron JM, Pruneda-Paz JL, Doherty CJ, Gross AM, Kang SE & Kay SA (2012) Arabidopsis circadian clock protein, TOC1, is a DNA-binding transcription factor. *Proc Natl Acad Sci USA* **109**, 3167–3172.
63 Pokhilko A, Fernndez AP, Edwards KD, Southern MM, Halliday KJ & Millar AJ (2012) The clock gene circuit in Arabidopsis includes a repressilator with additional feedback loops. *Mol Syst Biol* **8**, 574.
64 Huang W, Pérez-Garcíıa P, Pokhilko A, Millar AJ, Antoshechkin I, Riechmann JL & Mas P (2012) Mapping the core of the Arabidopsis circadian clock defines the network structure of the oscillator. *Science* **336**, 75–79.
65 Morant P-E, Thommen Q, Lemaire F, Vandermoere C, Parent B & Lefranc M (2009) Oscillations in the expression of a self-repressed gene induced by a slow transcriptional dynamics. *Phys Rev Lett* **102**, 068104.
66 Pfeuty B, Thommen Q & Lefranc M (2011) Robust entrainment of circadian oscillators requires specific phase response curves. *Biophys J* **100**, 2557–2565.
67 Gutenkunst RN, Waterfall JJ, Casey FP, Brown KS, Myers CR & Sethna JP (2007) Universally sloppy parameter sensitivities in systems biology models. *PLoS Comput Biol* **3**, e189.
68 Locke JCW, Westermark PO, Kramer A & Herzel H (2008) Global parameter search reveals design principles of the mammalian circadian clock. *BMC Syst Biol* **2**, 22.
69 Roenneberg T, Hut R, Daan S & Merrow M (2010) Entrainment concepts revisited. *J Biol Rhythms* **25**, 329–339.
70 Roenneberg T, Réemi J & Merrow M (2010) Modeling a circadian surface. *J Biol Rhythms* **25**, 340–349.
71 Akman OE, Guerriero ML, Loewe L & Troein C (2010) Complementary approaches to understanding the plant circadian clock. *Electron Proc Theor Comput Sci* **19**, 1–19.
72 Djouani-Tahri E, Motta J-P, Bouget F-Y & Corellou F (2010) Insights into the regulation of the core clock component TOC1 in the green picoeukaryote *Ostreococcus*. *Plant Signal Behav* **5**, 332–335.
73 Comas M, Beersma DGM, Spoelstra K & Daan S (2006) Phase and period responses of the circadian system of mice (*Mus musculus*) to light stimuli of different duration. *J Biol Rhythms* **21**, 362–372.
74 Tsumoto K, Kurosawa G, Yoshinaga T & Aihara K (2011) Modeling light adaptation in circadian clock: prediction of the response that stabilizes entrainment. *PLoS ONE* **6**, e20880.

75 Rand DA, Shulgin BV, Salazar JD & Millar AJ (2006) Uncovering the design principles of circadian clocks: mathematical analysis of flexibility and evolutionary goals. *J Theor Biol* **238**, 616–635.

76 Comas M, Beersma D, Hut R & Daan S (2008) Circadian phase resetting in response to light–dark and dark–light transitions. *J Biol Rhythms* **23**, 425–434.

77 O'Neill JS, van Ooijen G, Dixon LE, Troein C, Corellou F, Bouget F-Y, Reddy AB & Millar AJ (2011) Circadian rhythms persist without transcription in a eukaryote. *Nature* **469**, 554–558.

78 Geem ZW, Kim JH & Loganathan GV (2001) A new meta-heuristic algorithm for continuous engineering optimization: harmony search theory and practice. *Simulation* **76**, 60.

79 Moré J, Garbow B & Hillstrom K (1999) *MINPACK, version 1* [WWW document]. URL http://www.netlib.org/minpack/ [accessed on 15 January 2009].

80 Hairer E & Wanner G (1996) . *Solving Ordinary Differential Equations II. Stiff and Differential-Algebraic Problems. Springer Series in Computational Mathematics*, Vol.**14**. Springer-Verlag, Berlin.